Nonlinear optical studies of liquid crystal alignment on a rubbed polyvinyl alcohol surface

Xing Wei, Seok-Cheol Hong, Xiaowei Zhuang,* Tomohisa Goto,† and Y. R. Shen
Department of Physics, University of California, and Materials Sciences Division, Lawrence Berkeley National Laboratory, Berkeley, California 94720
(Received 5 January 2000)

Sum-frequency vibrational spectroscopy and second-harmonic generation have been used to measure the orientational distributions of the polymer chains and adsorbed 8CB liquid crystal molecules on a rubbed polyvinyl alcohol surface. Results show that the polymer chains at the surface appear to be well aligned by rubbing, and the adsorbed liquid crystal molecules are aligned, in turn, by the surface polymer chains. Strong correlation exists between the orientational distributions of the polymer chains and the liquid crystal molecules, indicating that the surface-induced bulk alignment of a liquid crystal film by rubbed polymer surfaces is via an orientational epitaxylike mechanism.

PACS number(s): 61.30.−v, 68.35.Bs, 78.30.Jw, 42.65.Ky

I. INTRODUCTION

The alignment of liquid crystal (LC) molecules on rubbed polymer surfaces was discovered in 1911 [1]. In recent years, this phenomenon has been studied extensively not only because of the basic interest in understanding the underlying mechanism, but also because of its relevance to LC display technology. Today, rubbed polymer films are widely used in industry to obtain homogeneous bulk LC alignment for LC displays [2]. Different mechanisms have been proposed for LC alignment on rubbed polymer surfaces. One assumes that rubbing creates microgrooves or scratches on polymer surfaces which then align LC along the grooves to minimize the energy of elastic distortion [3]. Another suggests that rubbing aligns surface polymer chains, which in turn align LC's through intermolecular interaction [4]. The latter is believed to be operative when LC molecules anchor strongly to polymer surfaces, as is commonly the case in the LC industry.

To study LC alignment by rubbed polymer surfaces, a number of experimental techniques have been used. Optical second-harmonic generation (SHG) showed that a rubbed polymer surface can align an adsorbed LC monolayer which then aligns the LC bulk by molecular correlation [5–8], providing convincing evidence that molecular interaction between a LC and a polymer at the surface is responsible for the LC alignment. Attempts to study the rubbed polymer itself with SHG have also been made, but the structural information obtained so far from SHG is rather limited [9]. Atomic force microscopy could provide images of rubbed polymer surfaces showing an overall anisotropy, but was unable to resolve the surface polymer chains [10–12]. Ellipsometry [13] and infrared spectroscopy [14–17] can measure rubbing-induced anisotropy and other structural changes in the polymer film. However, because of their lack of surface specificity, it is unclear whether these results indeed represent the real surface structure of the rubbed polymer. Grazing incidence x-ray scattering could probe a surface region of ~5 nm thick [18,19]. A higher surface sensitivity has been achieved by near-edge x-ray-absorption fine-structure (NEXAFS) spectroscopy which could probe a surface layer of ~1 nm thick [20–23].

In this paper, we describe the use of infrared-visible sum-frequency generation (SFG) vibrational spectroscopy to probe the structure of a rubbed polymer surface. SFG has been developed into a powerful surface analytical tool [24]. Similar to SHG, it is forbidden in media with inversion symmetry under the electric dipole approximation, but allowed at interfaces, where the inversion symmetry is broken. Therefore, it is ideally suited as a probe to study interfacial structure between two centrosymmetric media. Being a nonlinear optical process involving three optical waves, in principle, SFG can yield more detailed structural information than all the linear optical techniques including NEXAFS. We have applied SFG vibrational spectroscopy to rubbed polyvinyl alcohol (PVA, $[-CH_2\text{-}CHOH-]_n$). Rubbed PVA is known to align LC molecules in a way similar to rubbed polyimide [6], but has a much simpler monomer unit. We focus on the stretch vibrational modes of the CH_2 groups of PVA at the surface. The CH_2 groups directly associated with the PVA backbone are oriented perpendicularly to the local PVA chains, as shown in Fig. 1. From the measured SFG spectra,

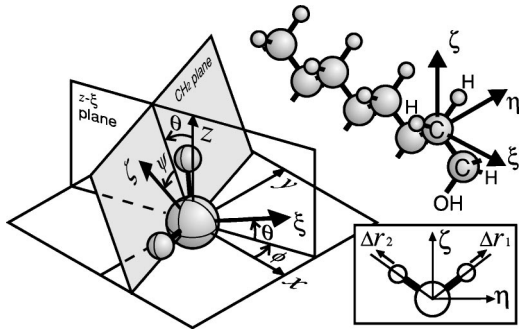

FIG. 1. Molecular structure of PVA and orientational geometry of a CH_2 group on a rubbed PVA surface. Axis x is along the rubbing direction, and z is along the surface normal of the polymer film. Axis ξ is normal to the CH_2 plane and along the PVA chain, ζ is along the symmetry axis of CH_2, and η is orthogonal to ξ and ζ.

*Present address: Department of Physics. Stanford University, Stanford, CA 94035-4060.

†Present address: Organic Material Research Laboratory, NEC Corporation, Kanagawa 216, Japan.

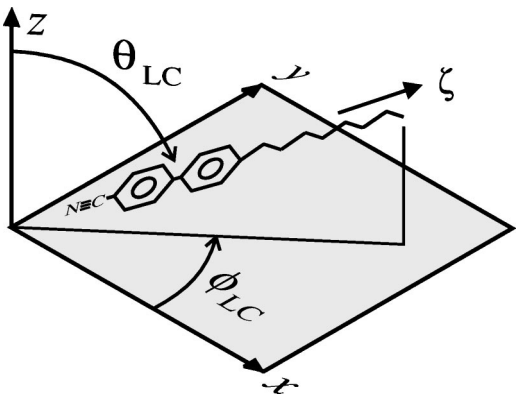

FIG. 2. Molecular structure and orientational coordinates of an 8CB molecule deposited on a rubbed PVA surface. ζ is along the long axis of the cyanobiphenyl core of the 8CB molecule. θ_{LC} and ϕ_{LC} are the polar and azimuthal angles of ζ. The x axis stands for the rubbing direction.

we can deduce an orientational distribution for the CH_2 groups at the surface. This then directly yields an orientational distribution for the PVA chains on the rubbed surface. We found that the PVA chain orientation is indeed strongly affected by rubbing. Results of this work were briefly reported in an earlier paper [25]. Here we present a detailed analysis of the SFG results together with the SHG study of an 8CB (4-*n*-octyl-4'-cyanobiphenyl) LC monolayer deposited on rubbed PVA (Fig. 2), showing how a rubbed PVA surface aligns the LC monolayer.

Section II provides the theoretical background for the work, and Sec. III describes the experimental arrangement. Experimental results and data analysis are presented in Sec. IV, and discussions of the results in Sec. V.

II. THEORY

A. Surface sum-frequency and second-harmonic generation

Surface SFG results from a second-order nonlinear polarization induced at an interface by two input fields $\mathbf{E}(\omega_1)$ and $\mathbf{E}(\omega_2)$ at frequencies ω_1 (visible) and ω_2 (infrared), respectively,

$$\mathbf{P}^{(2)}(\omega_s)=\epsilon_0\boldsymbol{\chi}^{(2)}:\mathbf{E}(\omega_1)\mathbf{E}(\omega_2), \tag{2.1}$$

where $\boldsymbol{\chi}^{(2)}$ denotes the surface nonlinear susceptibility tensor [26]. It can be shown that in MKS units the SFG output intensity in the reflected direction is given by [27]

$$I(\omega_s)=\frac{\omega_s^2}{8\epsilon_0 c^3\cos^2\beta_s}|\chi_{\mathrm{eff}}^{(2)}|^2 I(\omega_1)I(\omega_2). \tag{2.2}$$

Here β_s is the exit angle of the SF output, $I(\omega_i)$ is the beam intensity at ω_i, and $\chi_{\mathrm{eff}}^{(2)}$ is the effective surface nonlinear susceptibility defined as

$$\chi_{\mathrm{eff}}^{(2)}=[\mathbf{L}(\omega_s)\cdot\mathbf{e}_s]\cdot\boldsymbol{\chi}^{(2)}:[\mathbf{L}(\omega_1)\cdot\mathbf{e}_1][\mathbf{L}(\omega_2)\cdot\mathbf{e}_2], \tag{2.3}$$

with $\mathbf{e}_i$ being a unit polarization vector of the optical field at ω_i, and $\mathbf{L}(\omega_i)$ the tensorial Fresnel factor (See Appendix A for details).

Equations (2.1)–(2.3) also apply to second-harmonic generation with $\omega_1=\omega_2$. In SHG, often only one input laser beam at frequency ω (usually in the visible) is used and the SH signal at $\omega_s=2\omega$ is collected.

B. SFG vibrational spectroscopy for surface molecular groups

The nonlinear susceptibility tensor $\boldsymbol{\chi}^{(2)}(\omega_s=\omega_1+\omega_2)$ for SFG is expected to be resonantly enhanced when ω_2 approaches a surface vibrational resonance. Scanning over such resonances yields a surface SFG vibrational spectrum. We can express $\boldsymbol{\chi}^{(2)}$ in terms of the resonant nonlinear polarizability $\boldsymbol{\alpha}_{\mathrm{R}}^{(2)}$ for the surface molecular groups,

$$\boldsymbol{\chi}^{(2)}=\boldsymbol{\chi}_{\mathrm{NR}}^{(2)}+N_{\mathrm{S}}\langle\boldsymbol{\alpha}_{\mathrm{R}}^{(2)}\rangle_f=\boldsymbol{\chi}_{\mathrm{NR}}^{(2)}+N_{\mathrm{S}}\int\boldsymbol{\alpha}_{\mathrm{R}}^{(2)}(\Omega)f(\Omega)d\Omega, \tag{2.4}$$

where $\boldsymbol{\chi}_{\mathrm{NR}}^{(2)}$ describes the nonresonant contribution, N_{S} is the surface density of molecules, Ω denotes a set of orientational angles (θ,ϕ,ψ) defined in Fig. 1, and $\langle\ \rangle_f$ represents an orientational average over the orientational distribution function $f(\Omega)$.

We assume that $\boldsymbol{\alpha}_{\mathrm{R}}^{(2)}$ is composed of Lorentzian resonant terms,

$$\boldsymbol{\alpha}_{\mathrm{R}}^{(2)}(\omega_2)=\sum_q\frac{\mathbf{a}_q}{\omega_2-\omega_q+i\Gamma_q}, \tag{2.5}$$

where $\mathbf{a}_q$, ω_q, and Γ_q are the amplitude, resonant frequency and damping constant of the qth molecular vibrational mode. Insertion of Eq. (2.5) into Eq. (2.4) gives

$$\boldsymbol{\chi}^{(2)}(\omega_2)=\boldsymbol{\chi}_{\mathrm{NR}}^{(2)}+\sum_q\frac{\mathbf{A}_q}{\omega_2-\omega_q+i\Gamma_q}, \tag{2.6}$$

$$\mathbf{A}_q=N_{\mathrm{S}}\int\mathbf{a}_q(\Omega)f(\Omega)d\Omega. \tag{2.7}$$

Being a rank-3 tensor, $\boldsymbol{\chi}^{(2)}$ has in general 27 elements. Surface symmetry, however, can make some elements vanish and some become mutually dependent. In many cases, we can determine all the independent nonvanishing $\boldsymbol{\chi}^{(2)}$ elements by measuring $\chi_{\mathrm{eff}}^{(2)}$ with various beam geometries and polarization combinations. From the observed dispersion of $\boldsymbol{\chi}^{(2)}$ we can deduce $\mathbf{A}_q$ in Eq. (2.6). We can also obtain $\mathbf{a}_q$ in Eq. (2.5) for the molecular nonlinear polarizability $\boldsymbol{\alpha}_{\mathrm{R}}^{(2)}$ from other measurements or theoretical calculations. Then, Eq. (2.7) will allow us to obtain an approximate orientational distribution function $f(\Omega)$. Note that the microscopic local-field correction [28] is not included in Eqs. (2.4) and (2.7). As discussed in Appendix B, such correction has been partially included in the Fresnel factor L_{ZZ} by an empirical surface dielectric constant ϵ'.

Since we shall be interested in the stretch vibrations of the CH_2 groups of PVA, here we present a simple theoretical model to calculate the resonant mode amplitude $\mathbf{a}_q$ for CH_2. There are two stretch vibrational modes for a CH_2 group, namely, the symmetric (s) stretch and the antisymmetric (a) stretch. The theory of sum-frequency vibrational spectros-

copy shows that $\mathbf{a}_q$ is related to the infrared and Raman characteristics of a vibrational mode through the equation [29]

$$(a_q)_{lmn} = -\frac{1}{2\epsilon_0\omega_q}\frac{\partial\mu_n}{\partial Q_q}\frac{\partial\alpha^{(1)}_{lm}}{\partial Q_q}, \tag{2.8}$$

where $\partial\mu_n/\partial Q_q$ and $\partial\alpha^{(1)}_{lm}/\partial Q_q$ are the infrared dipole derivative and the Raman polarizability tensor of the qth vibrational mode, and Q_q is the classical normal coordinate. From Eq. (2.8) we can see some important properties of the tensor $\mathbf{a}_q$. First, the Raman polarizability tensor is symmetric for CH_2, and therefore $(a_q)_{lmn}$ is also symmetric in l and m, i.e., $(a_q)_{lmn}=(a_q)_{mln}$. Second, since all the $\partial\mu_n/\partial Q_q$ and $\partial\alpha^{(1)}_{lm}/\partial Q_q$ elements are real, $(a_q)_{lmn}$ must also be real, although $\boldsymbol{\chi}^{(2)}$ can be complex due to the damping constant Γ_q in Eq. (2.6).

We can use Eq. (2.8) to calculate $(a_q)_{lmn}$ for the two stretch modes of CH_2. If we assume that the carbon atom is fixed in position, the normal coordinates of the s and a stretch modes are

$$Q_{\mathrm{s}} = \sqrt{\frac{m_{\mathrm{H}}}{2}}(\Delta r_1+\Delta r_2),$$
$$Q_{\mathrm{a}} = \sqrt{\frac{m_{\mathrm{H}}}{2}}(\Delta r_1-\Delta r_2), \tag{2.9}$$

where Δr_1 and Δr_2 are the stretch distances of the two C-H bonds (Fig. 1), and m_{H} is the mass of a hydrogen atom. The dipole derivative $\partial\mu_n/\partial Q_q$ and the Raman polarizability $\partial\alpha^{(1)}_{lm}/\partial Q_q$ of these two modes can be calculated by assuming that the total dipole moment (or polarizability) is the sum of the dipole moments (or polarizabilities) of the two individual C-H bonds, and that the dipole moment (or polarizability) of each individual C-H bond depends only on its own coordinate. This bond additivity model has been used by other authors in similar calculations [30]. Using this model, we find

$$\frac{\partial\boldsymbol{\mu}}{\partial Q_{\mathrm{s}}} = \frac{1}{\sqrt{2m_{\mathrm{H}}}}\left(\frac{\partial\boldsymbol{\mu}_1}{\partial\Delta r_1}+\frac{\partial\boldsymbol{\mu}_2}{\partial\Delta r_2}\right),$$
$$\frac{\partial\boldsymbol{\mu}}{\partial Q_{\mathrm{a}}} = \frac{1}{\sqrt{2m_{\mathrm{H}}}}\left(\frac{\partial\boldsymbol{\mu}_1}{\partial\Delta r_1}-\frac{\partial\boldsymbol{\mu}_2}{\partial\Delta r_2}\right),$$
$$\frac{\partial\boldsymbol{\alpha}^{(1)}}{\partial Q_{\mathrm{s}}} = \frac{1}{\sqrt{2m_{\mathrm{H}}}}\left(\frac{\partial\boldsymbol{\alpha}^{(1)}_1}{\partial\Delta r_1}+\frac{\partial\boldsymbol{\alpha}^{(1)}_2}{\partial\Delta r_2}\right),$$
$$\frac{\partial\boldsymbol{\alpha}^{(1)}}{\partial Q_{\mathrm{a}}} = \frac{1}{\sqrt{2m_{\mathrm{H}}}}\left(\frac{\partial\boldsymbol{\alpha}^{(1)}_1}{\partial\Delta r_1}-\frac{\partial\boldsymbol{\alpha}^{(1)}_2}{\partial\Delta r_2}\right). \tag{2.10}$$

By symmetry, for the s stretch there are three independent nonvanishing $(a_{\mathrm{s}})_{lmn}$ elements $(a_{\mathrm{s}})_{\xi\xi\zeta}$, $(a_{\mathrm{s}})_{\eta\eta\zeta}$, and $(a_{\mathrm{s}})_{\zeta\zeta\zeta}$, and for the a stretch there is only one: $(a_{\mathrm{a}})_{\eta\zeta\eta}=(a_{\mathrm{a}})_{\zeta\eta\eta}$. Here (ξ,η,ζ) are the molecular coordinates defined in Fig. 1. To carry out numerical calculations, we need the values of the dipole and polarizability derivatives of a single C-H bond. Here we use the single bond dipole derivative deduced from Ref. [31] (the negative sign is based on the argument in Ref. [32]),

$$\frac{\partial\mu}{\partial\Delta r} \approx -0.86 \text{ De/Å} \approx -2.9\times10^{-20} \text{ C}, \tag{2.11}$$

and the single bond polarizability derivative from Ref. [33],

$$\frac{\partial\alpha^{(1)}_{\parallel}}{\partial\Delta r} \approx 3.0\times10^{-30} \text{ mC/V}, \tag{2.12}$$

$$\frac{\partial\alpha^{(1)}_{\perp}}{\partial\Delta r} \approx 0.14\times\frac{\partial\alpha^{(1)}_{\parallel}}{\partial\Delta r} \approx 0.4\times10^{-30} \text{ mC/V}. \tag{2.13}$$

After inserting these numbers into Eq. (2.8), we obtain all the nonvanishing $\mathbf{a}_q$ elements for the CH_2 stretch modes,

$$(a_{\mathrm{s}})_{\xi\xi\zeta}\approx 0.16\ a_0,$$
$$(a_{\mathrm{s}})_{\eta\eta\zeta}\approx 0.82\ a_0,$$
$$(a_{\mathrm{s}})_{\zeta\zeta\zeta}\approx 0.49\ a_0,$$
$$(a_{\mathrm{a}})_{\eta\zeta\eta}=(a_{\mathrm{a}})_{\zeta\eta\eta}\approx 0.66\ a_0, \tag{2.14}$$

where a_0 is a constant defined for a single C-H bond:

$$a_0 = -\frac{1}{2\epsilon_0\omega_q m_{\mathrm{H}}}\frac{\partial\mu}{\partial\Delta r}\frac{\partial\alpha^{(1)}_{\parallel}}{\partial\Delta r} \approx 5.3\times10^{-27} \text{ m}^4\,\text{V}^{-1}\,\text{sec}^{-1}. \tag{2.15}$$

C. SHG for a liquid crystal monolayer

SHG has been used successfully to measure the molecular orientational distributions of liquid crystal monolayers. A detailed description of the theory and technique can be found in Ref. [6]. Similar to SFG, the surface SHG nonlinear susceptibility is also an orientational average of the nonlinear polarizability of surface molecular groups.

For 8CB, the SHG nonlinear polarizability mainly originates from highly delocalized electrons in the cyanobiphenyl group, and has one dominant tensor element $\alpha^{(2)}_{\zeta\zeta\zeta}$ along the long molecular axis ζ (Fig. 2). As a good approximation [6], we can neglect other tensor elements of $\boldsymbol{\alpha}^{(2)}$, and express $\chi^{(2)}_{ijk}$ as

$$\chi^{(2)}_{ijk} = N_{\mathrm{S}}\langle(\hat{i}\cdot\hat{\xi})(\hat{j}\cdot\hat{\xi})(\hat{k}\cdot\hat{\xi})\rangle_g\alpha^{(2)}_{\zeta\zeta\zeta}$$
$$= N_{\mathrm{S}}\int(\hat{i}\cdot\hat{\xi})(\hat{j}\cdot\hat{\xi})(\hat{k}\cdot\hat{\xi})\alpha^{(2)}_{\zeta\zeta\zeta}g(\Omega)d\Omega, \tag{2.16}$$

where N_S is the surface number density of 8CB molecules; $\hat{i}$, $\hat{j}$, and $\hat{k}$ are the lab coordinates defined on the substrate; and $\langle\ \rangle_g$ denotes an average over the orientational distribution function $g(\Omega)$. By measuring all the nonvanishing independent $\chi^{(2)}_{ijk}$ elements we can deduce an approximate $g(\Omega)$.

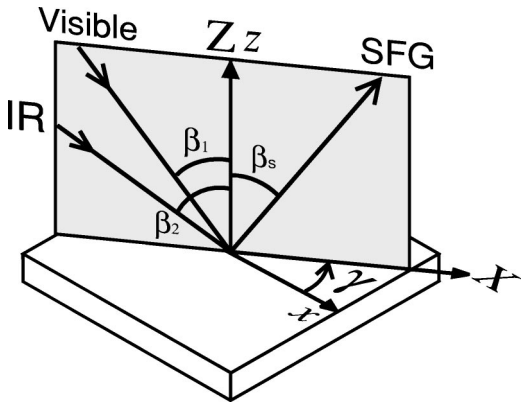

FIG. 3. Geometry of the incidence plane with respect to the sample surface in the SFG experiment. The rubbing direction is along *x*.

III. EXPERIMENT

Polyvinyl alcohol (Scientific Polymer Products, Inc., M.W.=14,000, 100% hydrolyzed) was dissolved in water (1.5% weight) and spin coated on fused quartz plates (hydrophilic), followed by baking and rubbing with velvet cloth. The film thickness was about 30 nm, and the rubbing strength used was at a saturation level, i.e., stronger rubbing would not improve the chain alignment further [6].

The SFG experimental setup has been described elsewhere [24]. In this experiment, a visible beam at 532 nm and an IR beam tunable from 2.6 to 3.7 μm to cover the CH stretch region (with a linewidth $\approx 6\,\mathrm{cm}^{-1}$), both having a 15-ps pulse width and a 20-Hz repetition rate, were overlapped at the sample with incidence angles $\beta_1 = 45°$ and $\beta_2 = 57°$, respectively (Fig. 3). The SFG output was detected in the reflected direction. The sample was mounted on a 360° rotational stage, and the SFG spectra were taken with various input-output polarization combinations and different sample orientations specified by the azimuthal angle γ between the incidence plane and the rubbing direction (Fig. 3).

In the SHG study of LC alignment on PVA, 8CB was deposited on a rubbed PVA surface by evaporation, and a visible laser beam at 532 nm was directed onto the sample with an incidence angle of 67° (see Ref. [6] for details). The SHG output was detected in the reflected direction. Four different input-output polarization combinations (s_{in}-s_{out}, s_{in}-p_{out}, p_{in}-s_{out}, and p_{in}-p_{out}) were used. The azimuthal variation of SHG was also measured.

IV. RESULTS AND ANALYSIS

A. SFG spectra and mode amplitudes

Surface SFG spectra in the CH stretch region of a rubbed PVA sample were taken with six different polarization combinations, each with different azimuthal orientations (typically every 45°). The spectra were found to be reproducible for different PVA samples prepared under the same conditions. Shown in Fig. 4 are the SFG spectra with the azimuthal angle $\gamma = 0°$ (parallel to rubbing) and $\gamma = 90°$ (perpendicular to rubbing) for the *ssp* (*s*-, *s*- and *p*-polarized SF output, visible input and infrared input, respectively), *sps* and *ppp* polarization combinations, and $\gamma = 90°$ for *sss*, *spp*, and *pps*. For comparison, the spectra of *ssp* and *sps* from an unrubbed PVA surface are shown in Fig. 5.

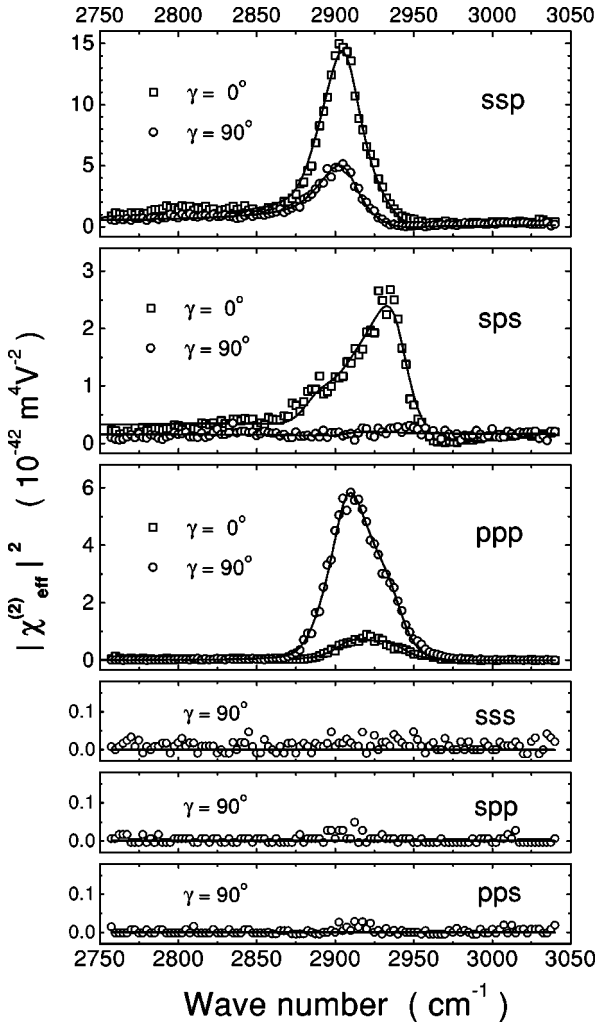

FIG. 4. SFG spectra of a rubbed PVA surface in the CH stretch range for different polarization combinations. Only spectra at $\gamma = 0°$ and 90° are shown for *ssp*, *sps*, and *ppp*. The spectra at $\gamma = 90°$ for *sss*, *spp*, and *pps* are dominated by noise. Solid curves are fits from Eq. (2.6).

All the measured SFG intensities have been calibrated with a reference *z*-cut quartz crystal (see Appendix C for details), yielding for each polarization combination and sample orientation a spectrum of $|\chi^{(2)}_{\mathrm{eff}}|^2$ in MKS units according to Eq. (2.2). All the $|\chi^{(2)}_{\mathrm{eff}}(\omega_2)|^2$ spectra can then be fit by

$$\chi^{(2)}_{\mathrm{eff}}(\omega_2) = \chi^{(2)}_{\mathrm{NR,eff}} + \sum_q \frac{A_{q,\mathrm{eff}}}{\omega_2 - \omega_q + i\Gamma_q}, \qquad (4.1)$$

assuming the presence of three resonant modes at $\omega_q/(2\pi c) = 2882$, 2907, and 2940 cm^{-1}, each with a damping constant $\Gamma/(2\pi c) = 16\,\mathrm{cm}^{-1}$. The first one, which is rather weak, probably comes from the stretch mode of the CH group on the PVA chain; the last two, highly prominent except for some polarization combinations and sample orientations, can be identified with the symmetric (*s*) and antisymmetric (*a*) stretch modes of CH_2 [34]. The azimuthal polar plots of the mode amplitudes $A_{s,\mathrm{eff}}$ and $A_{a,\mathrm{eff}}$ deduced by

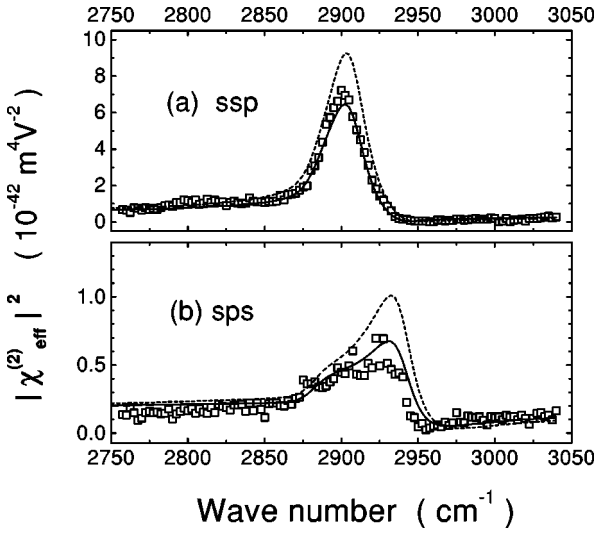

FIG. 5. SFG spectra of unrubbed PVA for different polarization combinations (a) *ssp* and (b) *sps*. The solid and dashed lines are theoretical predictions assuming different orientational distributions (see Sec. V B).

fitting of the spectra are presented in Fig. 6. Some additional data points of $A_{s,\mathrm{eff}}(ssp)$ and $A_{a,\mathrm{eff}}(sps)$ in Fig. 6 were deduced from the measured SFG peak intensity for every 5° with the infrared input frequency fixed on the resonant peak. $A_{s,\mathrm{eff}}(sps)$ is below the noise level, and not shown.

Note that the measurements described above could not determine the relative signs of $A_{q,\mathrm{eff}}$ for different polarization combinations. These relative signs, however, can be determined by measuring interference between different $A_{q,\mathrm{eff}}$ components. For example, the SFG intensity with *p*-polarized infrared input, mixed (*m*-, partially *s*- and partially *p*-) polarized visible input and *m*-polarized SFG output is proportional to the absolute square of the linear combination of $A_{q,\mathrm{eff}}(ssp)$ and $A_{q,\mathrm{eff}}(ppp)$, which can interfere constructively or destructively depending on their relative sign. From such interferences, we were able to determine the relative signs of all $A_{q,\mathrm{eff}}$. As shown in Fig. 6, if we choose the sign of $A_{s,\mathrm{eff}}(ssp)$ to be positive, we find $A_{a,\mathrm{eff}}(sps)$ and $A_{a,\mathrm{eff}}(ppp)$ positive, and $A_{a,\mathrm{eff}}(ssp)$ and $A_{s,\mathrm{eff}}(ppp)$ negative. Later, we will use these measured $A_{q,\mathrm{eff}}$ including their signs to deduce the tensor $\mathbf{A}_q$ through Eq. (2.3).

B. Surface specificity

In surface sum-frequency spectroscopy, there is always the question whether the SFG signal indeed comes from the surface under investigation [35]. In order to deduce surface structure from SFG spectra, one has to make sure that the SFG signal is dominated by the surface contribution.

For the rubbed PVA sample, the SFG signal might come from the bulk through electric-quadrupole and magnetic-dipole contributions, or from the interface between PVA and the fused quartz substrate. However, the fact that the SFG spectra of PVA are comparable in intensity to those observed from a closely packed monolayer of alkyl chains [37] indicates that the SFG signal of PVA originates from a monolayer of CH_2 pointing out of the polymer. The electric-quadrupole and magnetic-dipole contributions from CH_2 in the bulk are much weaker [36], and significant contribution from the polymer-quartz interface with CH_2 pointing toward the quartz side is unlikely because the quartz surface is hydrophilic [38]. Chemical studies indicate [39] that the monomer units in PVA ''prefer'' a head-to-tail arrangement, i.e., the OH groups are on alternate carbon atoms, and therefore all the CH_2 groups on a straight PVA chain should be on the same side of the chain, as illustrated in Fig. 1. Being hydrophobic, the CH_2 groups like to point out of the polymer surface. It is also known from infrared absorption studies [34] that strong hydrogen bonding exists between adjacent PVA chains. In order to maximize the number of hydrogen bonds to lower the surface free energy, the top layer of PVA

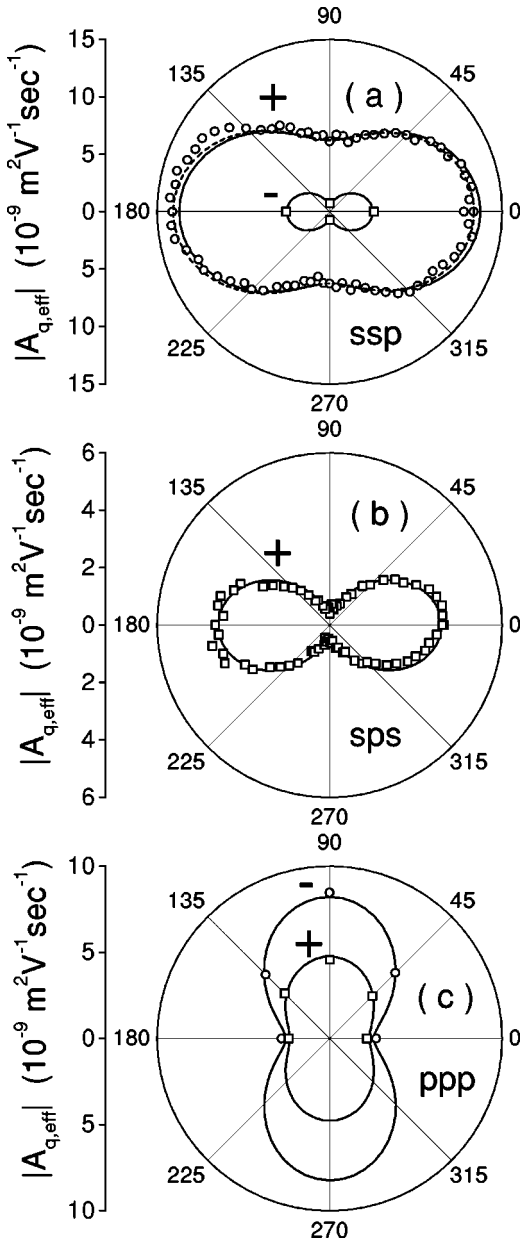

FIG. 6. Polar plots of the effective mode amplitudes $|A_{q,\mathrm{eff}}|$ of the CH_2 symmetric (circles) and antisymmetric (squares) stretch modes as functions of γ for different polarization combinations (a) *ssp*, (b) *sps*, and (c) *ppp*. The relative signs of $A_{q,\mathrm{eff}}$ are also shown in the figure. Symbols are values deduced from the measured SFG spectra. Lines are obtained from fits (see Sec. IV D).

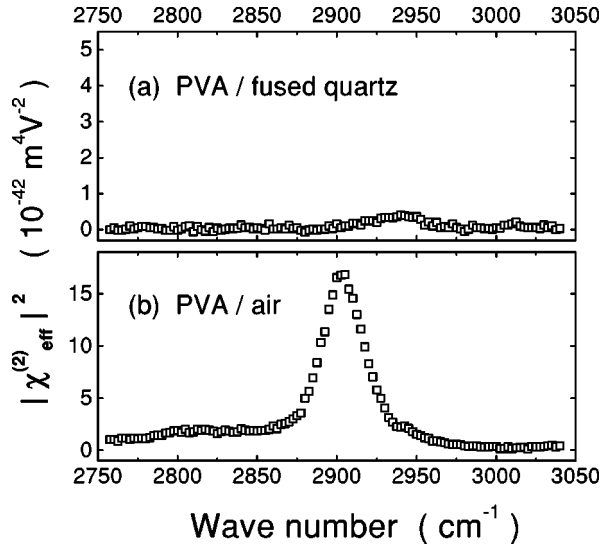

FIG. 7. The SFG spectra of two PVA samples measured through the fused quartz substrates. The SFG signal from (a) the thick PVA sample on fused quartz is dominated by the PVA–fused quartz interface, while the signal from (b) the thin spin-coated PVA film on fused quartz is dominated by the PVA-air interface. The polarization combination used is *ssp*. Note that the intensity of the spectrum from the PVA–air interface is higher than that in Fig. 5(a), because the Fresnel factors are different for the facing-down geometry.

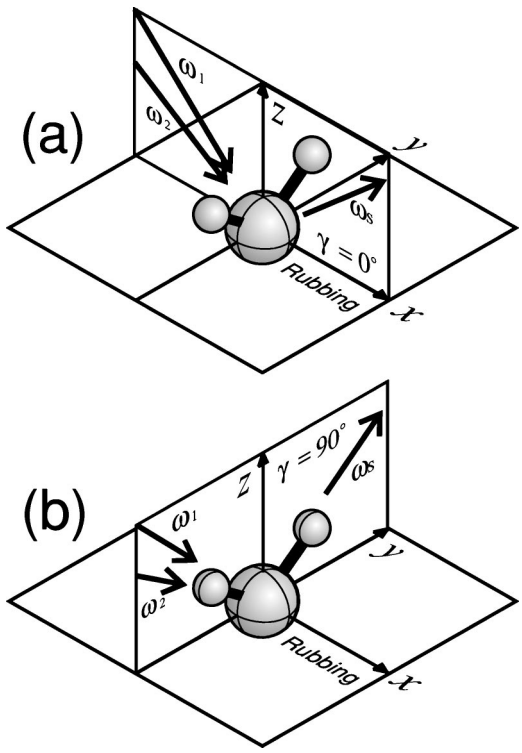

FIG. 8. Sketches showing that with the given CH_2 orientation, the beam geometry $\gamma=0°$ in (a) allows observation of the CH_2 *s* stretch mode by the *ssp* polarization combination, and the CH_2 *a* stretch mode by *sps*, in the SFG spectra, and the beam geometry $\gamma=90°$ in (b) allows observation of only the CH_2 *s*-stretch mode by the *ssp* polarization combination.

chains would orient their OH bonds into the bulk, and leave the CH_2 groups more or less polar ordered and pointing into air.

To check whether SFG from the PVA-air interface indeed dominated, we prepared a thick PVA sample ($\sim$500 μm) on a fused quartz substrate, and measured the reflected SFG spectrum through the fused quartz substrate with the PVA layer facing down. From this geometry, the SFG signal from the PVA-air interface is negligible because (1) the PVA surface on the air side is rough, and (2) the infrared input is completely attenuated by the thick PVA layer. The result is shown in Fig. 7, in comparison with the SFG spectrum from a thin ($\sim$30 nm) spin-coated PVA film (unrubbed) which was also measured through the fused quartz substrate. It clearly shows that the SFG contribution from the PVA–fused quartz interface is much weaker than that from the PVA–air interface.

We also measured the SFG spectrum of the thin PVA film through the fused quartz substrate, as we put the sample in contact with water, and found that the strong SFG signal disappeared. After drying the film, the spectrum reappeared, indicating that the PVA film had not been dissolved in water. This is in agreement with our understanding of the strong SFG signal from the PVA-air interface. With the sample in contact with water, strong hydrogen bonding between water and PVA would randomize the orientation of the surface CH_2 groups, causing a drastic decrease of the SFG intensity. Interestingly, this test experiment may also provide an example of environment-induced surface structural change of polymers, another important topic in polymer science and technology [40].

C. Qualitative analysis of the SFG spectra

Without any calculation, we can already obtain some qualitative information about the CH_2 orientation on the rubbed PVA surface. This is illustrated in Fig. 8.

First, the excitation of the CH_2 symmetric stretch requires an IR polarization component along the CH_2 symmetry axis ζ defined in Fig. 1. The fact that the mode is very strong for the *ssp* polarization combination (with the last index *p* being the infrared polarization), but very weak for the *sps* for all γ, indicates that the CH_2 axis ζ must be nearly along the *z* axis. Second, the excitation of the CH_2 antisymmetric stretch requires an IR component along the axis η in the CH_2 plane. Since this mode is very strong for *sps* at $\gamma=0°$ [Fig. 8(a)], but very weak at $\gamma=90°$ [Fig. 8(b)], the CH_2 plane must be nearly the *y*-*z* plane. Correspondingly, the PVA chains must be oriented nearly parallel to the surface along the *x* axis, the rubbing direction. Finally, as seen from the plot of $A_{s,\mathrm{eff}}(ssp)$ in Fig. 6, there is a small forward-backward asymmetry for $\gamma=0°$ and 180°. As will be shown below, this indicates that the average chain orientation has a slight upward tilt along the rubbing direction.

D. Quantitative analysis of the SFG data

As mentioned earlier, the surface nonlinear susceptibility $\chi^{(2)}_{ijk}$ (correspondingly, $(A_q)_{ijk}$ for each vibrational mode) has 27 matrix elements, but symmetry may greatly reduce the number of independent nonvanishing elements. First, because the rubbed PVA surface has C_{1v} symmetry with the

x-z plane being a mirror plane, all the $\chi^{(2)}_{ijk}$ elements with indices ijk containing an odd number of y should vanish. Second, as discussed in Sec. II B, we have the symmetry $\chi^{(2)}_{ijk}=\chi^{(2)}_{jik}$. Combining these two, we find that $(A_q)_{ijk}$ for each CH_2 mode has only ten independent nonvanishing elements with the following indices:

$$xxz, \quad yyz, \quad zzz, \quad xzx=zxx, \quad yzy=zyy,$$

$$xxx, \quad yyx, \quad zzx, \quad xyy=yxy, \quad xzz=zxz.$$

Furthermore, we note that the forward-backward asymmetry shown in Fig. 6 is very small, and that the SFG spectra for the sss, spp, and pps polarization combinations are too weak to distinguish from noise (Fig. 4). These suggest that we may first use C_{2v} as an approximation for the symmetry of the rubbed PVA surface, and neglect the last five matrix elements listed above which contain an odd number of x. With this approximation, we can deduce the five major (C_{2v} allowed) $(A_q)_{ijk}$ elements for both s and a stretches of CH_2. Later, the observed forward-backward asymmetry will be used to deduce some of the remaining (C_{2v} forbidden) elements if possible.

From the theory described in Sec. II, we find that $A_{q,\mathrm{eff}}$ in Eq. (4.1) is related to $(A_q)_{ijk}$ through

$$A_{q,\mathrm{eff}}=[\mathbf{L}(\omega_s)\cdot\mathbf{e}_s]\cdot\mathbf{A}_q:[\mathbf{L}(\omega_1)\cdot\mathbf{e}_1][\mathbf{L}(\omega_2)\cdot\mathbf{e}_2]. \quad (4.2)$$

Neglecting the forward-backward asymmetry, we can write $A_{q,\mathrm{eff}}$ for the three polarization combinations in terms of the five major $(A_q)_{ijk}$ elements:

$$A_{q,\mathrm{eff}}(\gamma,ssp)=\sin\beta_2 L_{YY}(\omega_s)L_{YY}(\omega_1)L_{ZZ}(\omega_2)\times[(A_q)_{yyz}\cos^2\gamma+(A_q)_{xxz}\sin^2\gamma], \quad (4.3)$$

$$A_{q,\mathrm{eff}}(\gamma,sps)=\sin\beta_1 L_{YY}(\omega_s)L_{ZZ}(\omega_1)L_{YY}(\omega_2)\times[(A_q)_{yzy}\cos^2\gamma+(A_q)_{xzx}\sin^2\gamma], \quad (4.4)$$

$$\begin{aligned}A_{q,\mathrm{eff}}(\gamma,ppp)&=-\cos\beta_s\cos\beta_1\sin\beta_2 L_{XX}(\omega_s)L_{XX}(\omega_1)L_{ZZ}(\omega_2)\times[(A_q)_{xxz}\cos^2\gamma+(A_q)_{yyz}\sin^2\gamma]\\&\quad+\sin\beta_s\sin\beta_1\sin\beta_2 L_{ZZ}(\omega_s)L_{ZZ}(\omega_1)L_{ZZ}(\omega_2)\times(A_q)_{zzz}.\end{aligned} \quad (4.5)$$

Here, for $A_{q,\mathrm{eff}}(\gamma,ppp)$, we have neglected the contributions from $(A_q)_{xzx}$, $(A_q)_{zxx}$, $(A_q)_{yzy}$, and $(A_q)_{zyy}$, which nearly cancel out themselves simply because $\beta_s\approx\beta_1$. All the Fresnel factors L_{ii} in Eqs. (4.3)–(4.5) can be calculated (Appendix A) except L_{ZZ}, in which the surface dielectric constant ϵ' is unknown (Appendix B). Therefore, with Eqs. (4.3)–(4.5), we can only determine the quantities

$$\frac{(A_q)_{xxz}}{\epsilon'(\omega_2)}, \quad \frac{(A_q)_{yyz}}{\epsilon'(\omega_2)}, \quad \frac{(A_q)_{zzz}}{\epsilon'(\omega_1)^2\epsilon'(\omega_2)},$$

TABLE I. Measured and calculated nonvanishing tensor elements A_{ijk} for the CH_2 symmetric (s) and antisymmetric (a) stretch modes. All values are in unit of $10^{-10}\,\mathrm{m^2\,V^{-1}\,sec^{-1}}$.

	s stretch		a stretch	
	measured	calculated	measured	calculated
A_{xxz}	225 ± 15	225	-30 ± 20	-12
A_{yyz}	475 ± 15	474	-135 ± 20	-146
A_{zzz}	345 ± 45	358	220 ± 70	158
$A_{xzx}=A_{zxx}$	~0	24	20 ± 25	52
$A_{yzy}=A_{zyy}$	~0	-31	230 ± 15	238
A_{xxx}	~0	-9	~0	-5
A_{yyx}	-19 ± 6	-19	~0	8
A_{zzx}	~0	-12	~0	-5
$A_{xyy}=A_{yxy}$	~0	3	~0	-9
$A_{xzz}=A_{zxz}$	~0	-8	~0	-5

$$\frac{(A_q)_{xzx}}{\epsilon'(\omega_1)}=\frac{(A_q)_{zxx}}{\epsilon'(\omega_1)}, \quad \frac{(A_q)_{yzy}}{\epsilon'(\omega_1)}=\frac{(A_q)_{zyy}}{\epsilon'(\omega_1)}$$

instead of $(A_q)_{ijk}$. Here, we have neglected the dispersion of ϵ' in the visible so that $\epsilon'(\omega_s)=\epsilon'(\omega_1)$. Using these five ''reduced'' $(A_q)_{ijk}$ elements as independent fitting parameters we can fit the experiment data well, as shown by the solid lines in Fig. 6, except for the forward-backward asymmetry of $A_{s,\mathrm{eff}}(ssp)$ which has been neglected so far.

In general we cannot separate $\epsilon'(\omega_i)$ from $(A_q)_{ijk}$ purely by SFG measurement. However, there exist the following equations relating some of the $(A_q)_{ijk}$ that are specific to the CH_2 stretch vibrations:

$$\begin{aligned}&(A_s)_{xxz}+(A_s)_{yyz}+(A_s)_{zzz}=N_S\langle\hat\zeta\cdot\hat z\rangle_f[(a_s)_{\xi\xi\zeta}+(a_s)_{\eta\eta\zeta}+(a_s)_{\zeta\zeta\zeta}],\\&(A_s)_{xzx}+(A_s)_{yzy}+(A_s)_{zzz}=N_S\langle\hat\zeta\cdot\hat z\rangle_f(a_s)_{\zeta\zeta\zeta},\\&(A_a)_{xxz}+(A_a)_{yyz}+(A_a)_{zzz}=0,\\&(A_a)_{xzx}+(A_a)_{yzy}+(A_a)_{zzz}=N_S\langle\hat\zeta\cdot\hat z\rangle_f(a_a)_{\eta\zeta\eta}.\end{aligned} \quad (4.6)$$

The derivation of Eq. (4.6) can be found in Appendix D. These additional equations of constraint allow us to deduce $\epsilon'(\omega_i)$ from experiment without knowing the actual orientational distribution of the CH_2 groups. Applying Eq. (4.6) to the five ''reduced'' $(A_q)_{ijk}$ elements deduced from experiment, we find $\epsilon'(\omega_1)=2.1$ and $\epsilon'(\omega_2)=1.5$. We can then obtain the five corresponding $(A_q)_{ijk}$ elements; their values are listed in Table I and labeled as ''measured.''

Finally we include the forward-backward asymmetry observed in the SFG spectra for the ssp polarization combination. Including contributions from $(A_q)_{yyx}$ and $(A_q)_{xxx}$, Eq. (4.3) becomes

$$A_{q,\mathrm{eff}}(\gamma,ssp)=\sin\beta_2 L_{YY}(\omega_s)L_{YY}(\omega_1)L_{ZZ}(\omega_2)\times[(A_q)_{yyz}\cos^2\gamma+(A_q)_{xxz}\sin^2\gamma]+\cos\beta_2 L_{YY}(\omega_s)L_{YY}(\omega_1)L_{XX}(\omega_2)\times[(A_q)_{yyx}\cos^3\gamma+(A_q)_{xxx}\cos\gamma\sin^2\gamma]. \tag{4.7}$$

It turns out that $(A_s)_{yyx}$ is the only additional element that can be determined with sufficient accuracy. The dashed line in Fig. 6(a) is the fit with a non-zero $(A_s)_{yyz}$. The deduced value of $(A_s)_{yyx}$ is listed in Table I.

With these measured values of $(A_q)_{ijk}$, we can then use Eqs. (2.7) and (2.14) to obtain an approximate orientational distribution function $f(\theta,\phi,\psi)$ for the CH_2 groups. Knowing that the PVA chains are quite well aligned, we can assume a Gaussian distribution

$$f(\theta,\phi,\psi)=C\exp\left[-\frac{(\theta-\theta_0)^2}{2\sigma_\theta^2}-\frac{(\phi-\phi_0)^2}{2\sigma_\phi^2}-\frac{(\psi-\psi_0)^2}{2\sigma_\psi^2}\right], \tag{4.8}$$

where C is a normalization constant; $\phi_0=\psi_0=0°$ by symmetry; and θ_0, σ_θ, σ_ϕ, and σ_ψ are parameters to be determined. For this calculation, the distribution function $f(\theta,\phi,\psi)$ is defined such that the probability of finding a CH_2 group oriented at (θ',ϕ',ψ') in the range $\theta<\theta'<\theta+d\theta$, $\phi<\phi'<\phi+d\phi$, and $\psi<\psi'<\psi+d\psi$ is equal to $f(\theta,\phi,\psi)d\theta d\phi d\psi$. We find, for the best fit,

$$\theta_0=2.5°\pm0.7°,$$

$$\sigma_\theta=26°\pm5°,$$

$$\sigma_\phi=27°\pm5°,$$

$$\sigma_\psi=35°\pm5°.$$

These values, when used with Eq. (4.8) in Eq. (2.7) to calculate $(A_q)_{ijk}$, reproduce almost all the measured $(A_q)_{ijk}$ values within the experimental error, as shown in the column ''calculated'' in Table I. One may notice that the number of experimentally deduced $(A_q)_{ijk}$ far exceeds the number of input parameters [θ_0, σ_θ, σ_ϕ, σ_ψ, $\epsilon'(\omega_1)$, $\epsilon'(\omega_2)$, and N_S] used for this calculation. The fact that we can still consistently reproduce all the measured $(A_q)_{ijk}$ values indicates that Eq. (4.8) is a good representation of the orientational distribution.

The above results focus on the surface CH_2 groups. Since the CH_2 molecular plane is perpendicular to the PVA chain locally, the same set of parameters θ and ϕ also describe the orientation of the polymer chains. The values listed above indicate that the PVA chains lie almost flat and are well aligned on the surface with an average 2.5° upward tilt along the rubbing direction.

E. SHG study of 8CB monolayer on rubbed PVA

As described in Sec. II C, the molecular orientational distribution of an 8CB monolayer adsorbed on a rubbed polymer surface can be determined from SHG measurements.

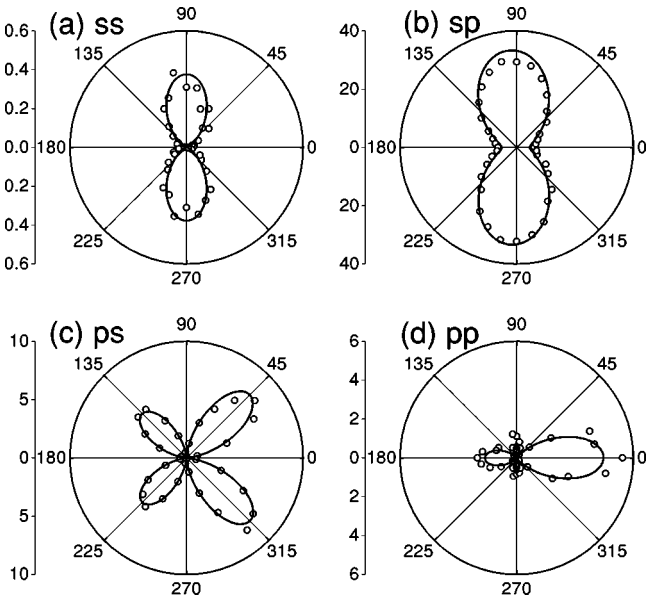

FIG. 9. Polar plots of SHG intensities (arbitrary units) from an 8CB monolayer on a rubbed PVA surface. 0° and 180° are the rubbing and antirubbing directions, respectively. Circles are the experiment data and solid lines are the theoretical fits. The input-output polarization combinations are (a) s_{in}-s_{out}; (b) s_{in}-p_{out}, (c) p_{in}-s_{out}, and (d) p_{in}-p_{out}.

Deposition of the 8CB monolayer was monitored by SHG as an *in situ* probe [41]. In Fig. 9 we present the SHG intensities from the 8CB monolayer on rubbed PVA as a function of the sample azimuthal angle γ for different input-output polarization combinations.

The 8CB monolayer on rubbed PVA also has a macroscopic C_{1v} symmetry, which restricts the number of nonvanishing independent $\chi^{(2)}_{ijk}$ elements to six under the approximation that $\alpha_{\zeta\zeta\zeta}$ dominates over other nonvanishing elements of $\boldsymbol{\alpha}^{(2)}$ of 8CB. As listed in Ref. [6], they are

$$\chi^{(2)}_{zzz},$$

$$\chi^{(2)}_{xxx},$$

$$\chi^{(2)}_{xyy}=\chi^{(2)}_{yxy}=\chi^{(2)}_{yyx},$$

$$\chi^{(2)}_{xzz}=\chi^{(2)}_{zxz}=\chi^{(2)}_{zzx},$$

$$\chi^{(2)}_{zxx}=\chi^{(2)}_{xzx}=\chi^{(2)}_{xxz},$$

$$\chi^{(2)}_{zyy}=\chi^{(2)}_{yzy}=\chi^{(2)}_{yyz},$$

and can be deduced by fitting the data in Fig. 9 using Eqs. (2.2) and (2.3). The fit is plotted as solid lines in Fig. 9, and the deduced nonvanishing $\chi^{(2)}_{ijk}$ elements are presented in Table II.

As in Ref. [6], we can assume for 8CB molecules in the monolayer an orientational distribution of the form

$$g(\theta_{\mathrm{LC}},\phi_{\mathrm{LC}})=C\exp\left[-\frac{(\theta_{\mathrm{LC}}-\theta_{\mathrm{LC},0})^2}{2\sigma^2}\right][1+d_1\cos\phi_{\mathrm{LC}}+d_2\cos(2\phi_{\mathrm{LC}})+d_3\cos(3\phi_{\mathrm{LC}})], \tag{4.9}$$

TABLE II. Nonvanishing independent $\chi^{(2)}_{ijk}$ elements of the 8CB monolayer on rubbed PVA deduced from the SHG experiment, with the zzz component normalized to 1.

$\chi^{(2)}_{zzz}/\epsilon'^3$	1
$\chi^{(2)}_{xxx}$	3.0 ± 0.5
$\chi^{(2)}_{xyy}$	0.32 ± 0.25
$\chi^{(2)}_{xzz}/\epsilon'^2$	0.15 ± 0.09
$\chi^{(2)}_{zxx}/\epsilon'$	11.5 ± 0.8
$\chi^{(2)}_{zyy}/\epsilon'$	4.4 ± 0.4

where θ_{LC} and ϕ_{LC} are the polar and the azimuthal angles defined in Fig. 2 , and $\theta_{LC,0}$, σ, d_1, d_2, and d_3 are five independent parameters to be determined from the five measured ratios in Table II using Eq. (2.16) with a given value of ϵ'. The results are presented in Table III. In this case, ϵ' cannot be determined separately, and the assumption $\epsilon'(\omega)=\epsilon'(2\omega)$ used here also may not be true because of the electronic resonance of 8CB molecules at the second-harmonic frequency. Nevertheless, as shown in Table III, varying ϵ' from 1 to 2.25 mainly changes the deduced values of $\theta_{LC,0}$ and σ, and has little effect on the parameters d_1, d_2, and d_3 which describe the azimuthal distribution.

V. DISCUSSIONS

A. Surface density of CH_2 groups

As seen in Eq. (2.7), N_S, the surface density of CH_2 groups, is a parameter needed in our quantitative analysis of the SFG data. To obtain the best-fit values of $(A_q)_{ijk}$ listed in the ''calculated'' column in Table I, we used

$$N_S=(1.7\pm0.2)\times10^{15}\ \text{cm}^{-2}, \tag{5.1}$$

which seems too large considering that the CH_2 surface density calculated from the PVA crystalline structure [42] is only about $7\times10^{14}\,\text{cm}^{-2}$. This is presumably because in our calculation we have neglected the factor $l_\parallel(\omega_s)l_\parallel(\omega_1)l_\parallel(\omega_2)$ resulting from the microscopic local-field effect. As discussed in Appendix B, N_S in Eq. (2.7) should be replaced by $N_S l_\parallel(\omega_s)l_\parallel(\omega_1)l_\parallel(\omega_2)$. References [43,44] show that $l_\parallel$ is usually larger than 1, which makes the value of N_S closer to the expected one.

B. Effect of rubbing on PVA surface structure

We have presented the SFG spectra of the ssp and sps polarization combinations for the unrubbed PVA sample (Fig. 5). The spectra from the rubbed and unrubbed samples look similar except that there is no azimuthal spectral variation for the unrubbed one. The dashed lines in Fig. 5 are predicted spectra for the unrubbed sample assuming the same Gaussian distribution for θ and ψ deduced earlier for the rubbed one, but a uniform distribution in ϕ. The absolute intensities of the measured spectra are slightly lower than predicted. A somewhat broader distribution in θ and ψ ($\sigma_\theta=35°$, $\sigma_\psi=45°$) fits the spectra well (solid lines).

TABLE III. Deduced parameters in $g(\theta_{LC},\phi_{LC})$ for various surface dielectric constant ϵ' of the 8CB monolayer.

ϵ'	θ_0 (deg)	σ (deg)	d_1	d_2	d_3
1.0	80 ± 5	6 ± 3	$0.07\pm.03$	$0.85\pm.03$	$0.04\pm.02$
1.25	78 ± 6	8 ± 4	$0.07\pm.03$	$0.85\pm.03$	$0.04\pm.02$
1.5	75 ± 8	9 ± 4	$0.07\pm.03$	$0.85\pm.03$	$0.04\pm.02$
1.75	72 ± 9	10 ± 5	$0.07\pm.03$	$0.85\pm.03$	$0.04\pm.02$
2.0	69 ± 10	11 ± 5	$0.07\pm.03$	$0.85\pm.03$	$0.04\pm.02$
2.25	66 ± 12	12 ± 6	$0.07\pm.03$	$0.85\pm.03$	$0.04\pm.02$

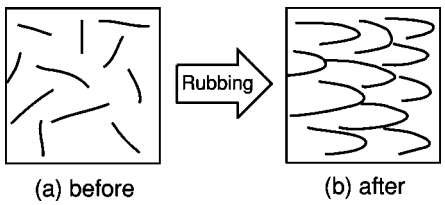

FIG. 10. Proposed polymer chain distribution (top view) on a PVA surface (a) before and (b) after rubbing.

Based on these results, a possible scenario of rubbing induced PVA chain ordering is proposed in Fig. 10. Before rubbing, some sections of the PVA chains were lying more or less flat on the surface and isotropic in the plane, with their ends presumably buried in the bulk. During rubbing, fibers on the rubbing material would grab the surface polymer chains, stretch them in the rubbing direction and even pull some chain sections out from the subsurface, resulting in stacked elongated half loops one on top of another. This would explain not only the azimuthal chain ordering in the rubbing direction, but also the forward-backward asymmetry.

C. Molecular interaction between 8CB and PVA

From the SFG and SHG studies we have obtained the orientational distribution functions $f(\theta,\phi,\psi)$ for the surface PVA chains and $g(\theta_{LC},\phi_{LC})$ for the molecules in the 8CB monolayer independently. It is important to find the correlation between them. In order to do so, we calculate a grand azimuthal distribution function $F(\phi)$ for PVA chains by integrating $f(\theta,\phi,\psi)$ over θ and ψ, and also $G(\phi_{LC})$ for the 8CB molecules by integrating $g(\theta_{LC},\phi_{LC})$ over θ_{LC}. However, we note that unlike an 8CB molecule, a section of PVA chain has no polarity, i.e., (θ,ϕ) and $(-\theta,\phi+180°)$ describe the same chain orientation. To define $f(\theta,\phi,\psi)$ over all orientations, we can limit θ between 0° and 90° and vary ϕ over the entire 360°. We naturally use the same limiting ranges for θ_{LC} and ϕ_{LC} to define $g(\theta_{LC},\phi_{LC})$ for polar 8CB molecules.

A polar plot of $\sqrt{F(\phi)}$ and $\sqrt{G(\phi_{LC})}$ are presented in Fig. 11. The correlation between the two is remarkable. As we expected, the rubbed PVA surface appears to be more ordered in the azimuthal distribution than the adsorbed 8CB monolayer. This suggests that the rubbed polymer surface indeed serves as a molecular template to align LC molecules through short-range molecular interaction [45].

The forward-backward asymmetry of the 8CB orientational distribution (represented by the positive coefficient $d_1=0.07$) indicates that the 8CB molecules prefer to align in the forward direction. This must be somehow related to the average upward tilt angle ($\theta_0=2.5°$) of the PVA chains.

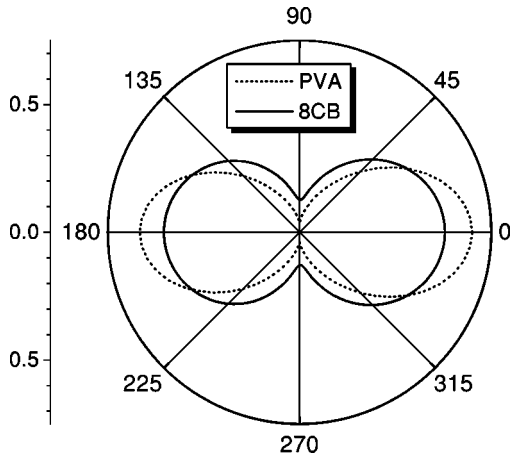

FIG. 11. Polar plot of the grand azimuthal distribution functions of the PVA chains (dashed line) and 8CB molecules (solid line) on a rubbed PVA surface. Square root values are used, so that the total areas inside the two curves remain constant.

Similar results have also been found from other rubbed polymers [16,21,22], yet no theoretical model is available to correlate these two tilt angles quantitatively. There are, however, some qualitative explanations. For example, it was assumed that rubbing induces a saw-tooth-like polymer surface which leads to a homogeneous LC alignment with a forward pretilt angle [46]. This is consistent with the scenario we proposed for the rubbed PVA surface (Fig. 10), in which the 8CB molecules adsorbed on the back-slanted terraces would appear to align more in the forward direction. As demonstrated in Ref. [8], the LC monolayer then governs the forward pretilt angle of a bulk LC film.

VI. CONCLUSION

We have used SFG surface vibrational spectroscopy to determine a quantitative orientational distribution of the polymer chains at the very top surface of a rubbed PVA sample. We have also used SHG to determine the orientational distribution of a monolayer of 8CB molecules adsorbed on rubbed PVA. Comparison of the two in the azimuthal plane shows that they are well correlated. This strongly supports the belief that ''orientational epitaxy'' is the mechanism responsible for the surface-induced LC bulk alignment by rubbed polymer surfaces. We have proposed a possible scenario on how rubbing changes the polymer chain conformation at the surface, which is subject to future experimental tests. This work is also a demonstration to show that SFG vibrational spectroscopy can be an effective tool to probe quantitatively the surface structure of a polymer, with or without external perturbation.

ACKNOWLEDGMENTS

The authors gratefully acknowledge Dr. A. I. Lvovsky's help in the numerical calculations. This work was supported by the NSF through Grant No. DMR-9704384.

APPENDIX A: FRESNEL FACTORS

The Fresnel factors of an interface between two continuous media with dielectric constants ϵ_1 and ϵ_2 are [24]

TABLE IV. Some parameters of the three beams and the calculated Fresnel factors for the air–fused quartz interface (applicable to the top surface only).

	ω_s	ω_1	ω_2
λ	460 nm	532 nm	3.4 μm
n	1.465	1.461	1.410
β	46.5°	45°	57°
L_{XX}	0.93	0.92	1.02
L_{YY}	0.70	0.71	0.65
L_{ZZ}	$1.07/\epsilon_s'$	$1.08/\epsilon_1'$	$0.98/\epsilon_2'$
$e_X L_{XX}(p)$	-0.64	0.65	0.56
$e_Y L_{YY}(s)$	0.70	0.71	0.65
$e_Z L_{ZZ}(p)$	$0.78/\epsilon_s'$	$0.77/\epsilon_1'$	$0.82/\epsilon_2'$

$$L_{XX}(\omega_i)=\frac{2\epsilon_1(\omega_i)k_{2Z}(\omega_i)}{\epsilon_2(\omega_i)k_{1Z}(\omega_i)+\epsilon_1(\omega_i)k_{2Z}(\omega_i)},$$

$$L_{YY}(\omega_i)=\frac{2k_{1Z}(\omega_i)}{k_{1Z}(\omega_i)+k_{2Z}(\omega_i)}, \tag{A1}$$

$$L_{ZZ}(\omega_i)=\frac{2\epsilon_1(\omega_i)\epsilon_2(\omega_i)k_{1Z}(\omega_i)}{\epsilon_2(\omega_i)k_{1z}(\omega_i)+\epsilon_1(\omega_i)k_{2Z}(\omega_i)}\frac{1}{\epsilon'(\omega_i)},$$

where $\epsilon'(\omega_i)$ is an empirical dielectric constant of the surface monolayer at ω_i. The physical meaning of $\epsilon'(\omega_i)$ will be discussed in Appendix B.

The Fresnel factors for the surface of a thin film coated on a substrate are slightly more complicated. Details can be found in the appendixes of Ref. [6]. In this experiment, the coated PVA film turns out to have little effect on the Fresnel factors because the thickness of the PVA film is only ~ 30 nm, much less than an optical wavelength, and the refractive index of PVA is not too different from that of the fused quartz substrate. Therefore we can use the calculated Fresnel factors listed in Table IV for the air–fused quartz interface as a good approximation.

APPENDIX B: DIELECTRIC CONSTANT OF THE SURFACE LAYER

In the theory of surface nonlinear optical spectroscopy we have introduced a dielectric constant ϵ' for the surface layer, which appears in the Fresnel factor L_{ZZ} in Eq. (A1). From the theoretical point of view, the dielectric constant is not well defined for a monolayer because it is a macroscopic or mesoscopic property. However, we realize that ϵ' can be interpreted as a result of the microscopic local-field correction in a monolayer [43,44], which needs to be addressed here.

We consider a surface monolayer of molecules at an interface between two media with dielectric constants ϵ_1 and ϵ_2. The local-field components experienced by these molecules are

$$E_X^{(\mathrm{Loc})}=l_{XX}L_{XX}E_X,$$

$$E_Y^{(\mathrm{Loc})}=l_{YY}L_{YY}E_Y, \tag{B1}$$

$$E_Z^{(\mathrm{Loc})}=l_{ZZ}L_{ZZ}E_Z,$$

where l_{ii} denotes the microscopic local-field correction factor, L_{ii} is the Fresnel or macroscopic local-field factor [defined by Eq. (A1) but without the factor $1/\epsilon'$], and E_i is the electric field component of the incoming and outgoing optical plane waves. If $l_{XX}=l_{YY}=l_{\parallel}$ and $l_{ZZ}=l_{\perp}$, the total local-field factors including both macroscopic and microscopic effects are

$$F_{XX}=l_{XX}L_{XX}=l_{\parallel}\frac{2\epsilon_1 k_{2Z}}{\epsilon_2 k_{1Z}+\epsilon_1 k_{2Z}},$$

$$F_{YY}=l_{YY}L_{YY}=l_{\parallel}\frac{2k_{1Z}}{k_{1Z}+k_{2Z}}, \tag{B2}$$

$$F_{ZZ}=l_{ZZ}L_{ZZ}=l_{\perp}\frac{2\epsilon_1\epsilon_2 k_{1Z}}{\epsilon_2 k_{1Z}+\epsilon_1 k_{2Z}},$$

which should be used in Eq. (2.3) instead of L_{ii}. We notice that F_{ii} differs from L_{ii} in Eq. (A1) only by a common factor $l_{\parallel}$ if we define

$$\epsilon'=\frac{l_{\parallel}}{l_{\perp}}. \tag{B3}$$

It has been shown that the value of ϵ' defined this way is usually between 1 and the bulk dielectric constant ϵ [44]. The physical meaning of ϵ' now becomes clear; it is simply the ratio of $l_{\parallel}$ and $l_{\perp}$. By introducing the factor $1/\epsilon'$ in Eq. (A1), we have partially included the microscopic local-field correction. To have it fully included, Eq. (2.4) should be changed to

$$\boldsymbol{\chi}^{(2)}=\boldsymbol{\chi}^{(2)}_{\mathrm{NR}}+N_S l_{\parallel}(\omega_s)l_{\parallel}(\omega_1)l_{\parallel}(\omega_2)\langle\boldsymbol{\alpha}^{(2)}_{\mathrm{R}}\rangle_f, \tag{B4}$$

and Eq. (2.7) becomes

$$\mathbf{A}_q=N_S l_{\parallel}(\omega_s)l_{\parallel}(\omega_1)l_{\parallel}(\omega_2)\int \mathbf{a}_q(\Omega)f(\Omega)d\Omega. \tag{B5}$$

Such additional correction modifies the surface density N_S by a constant $l_{\parallel}(\omega_s)l_{\parallel}(\omega_1)l_{\parallel}(\omega_2)$, but has no effect on our deduction of the distribution function $f(\Omega)$.

APPENDIX C: EFFECTIVE SURFACE NONLINEAR SUSCEPTIBILITY OF CRYSTALLINE QUARTZ

Equation (2.2) shows that we can measure $|\chi^{(2)}_{\mathrm{eff}}|^2$ of a sample by comparing its SFG intensity with that from a standard reference sample with a known $\chi^{(2)}_{\mathrm{eff}}$. In this experiment, we used a z-cut α-SiO_2 (quartz) crystal as our reference sample. The SFG signal from crystalline quartz is mainly from the bulk, which has D_3 symmetry with the nonvanishing $\chi^{(2)}_{ijk}$ elements

$$\chi^{(2)}_{xxx}=-\chi^{(2)}_{xyy}=-\chi^{(2)}_{yyx}=-\chi^{(2)}_{yxy},$$

$$\chi^{(2)}_{xyz}=-\chi^{(2)}_{yxz},$$

$$\chi^{(2)}_{xzy}=-\chi^{(2)}_{yzx},$$

$$\chi^{(2)}_{zxy}=-\chi^{(2)}_{zyx},$$

among which $\chi^{(2)}_{xxx}$ (defined as $\chi^{(2)}_{\mathrm{q}}$ below), and those equal to $\chi^{(2)}_{xxx}$ are much larger than the others [47]. In the following calculation we neglect the weaker ones. Formal solution of the reflected SFG amplitude from a medium with bulk nonlinear susceptibility can be found in Ref. [48]. Applying it to a z-cut quartz crystal shows that the SFG intensity is maximized when the x axis of the crystal is in the incidence plane, and the absolute values of the effective surface nonlinear susceptibilities are

$$|\chi^{(2)}_{\mathrm{eff}}(ssp)|=g\cos\beta_2 L_{YY}(\omega_s)L_{YY}(\omega_1)L_{XX}(\omega_2)\chi^{(2)}_{\mathrm{q}}l_c,$$

$$|\chi^{(2)}_{\mathrm{eff}}(sps)|=g\cos\beta_1 L_{YY}(\omega_s)L_{XX}(\omega_1)L_{YY}(\omega_2)\chi^{(2)}_{\mathrm{q}}l_c, \tag{C1}$$

$$|\chi^{(2)}_{\mathrm{eff}}(ppp)|=g\cos\beta_s\cos\beta_1\cos\beta_2 \times L_{XX}(\omega_s)L_{XX}(\omega_1)L_{XX}(\omega_2)\chi^{(2)}_{\mathrm{q}}l_c.$$

Here, β_i and L_{ii} are the incidence angle and Fresnel factor, both listed in Table V, l_c is the effective coherence length for the reflected SFG, and $g=2$ is a degeneracy constant which arises from the number of distinguishable permutations of the input frequencies [47]. We should mention here that in our usual definition of surface nonlinear susceptibility $\chi^{(2)}_{ijk}$ for sum-frequency vibrational spectroscopy, this factor of $g=2$ has already been included. In other words, we do not distinguish between $\chi^{(2)}_{ijk}(\omega_s=\omega_1+\omega_2)$ and $\chi^{(2)}_{ikj}(\omega_s=\omega_2+\omega_1)$. In the present experiment,

TABLE V. Parameters used to calculated $\chi^{(2)}_{\mathrm{eff}}$ of a z-cut quartz crystal. For convenience the birefringence of the crystal is neglected, and the refractive index of the ordinary wave n_o is used for all polarizations.

	ω_s	ω_1	ω_2
λ	460 nm	532 nm	3.4 μm
$n=n_o$	1.553	1.547	1.49
β	46.5°	45°	57°
L_{XX}	0.90	0.90	1.01
L_{YY}	0.67	0.68	0.61

$$l_c=\frac{1}{k_{2z}(\omega_s)+k_{2z}(\omega_1)+k_{2z}(\omega_2)}=\frac{1}{2\pi\left(\frac{\sqrt{n(\omega_s)^2-\sin^2\beta_s}}{\lambda_s}+\frac{\sqrt{n(\omega_1)^2-\sin^2\beta_1}}{\lambda_1}+\frac{\sqrt{n(\omega_2)^2-\sin^2\beta_2}}{\lambda_2}\right)}\approx 27 \text{ nm}. \tag{C2}$$

Since in our experiment, SFG from crystalline quartz is far from resonances, we may neglect dispersion and take

$$\chi_q^{(2)}=2d_{11}\approx 8.0\times 10^{-13} \text{ m/V}, \tag{C3}$$

where d_{11} refers to the nonlinear coefficient for SHG, and its value for $\lambda=1.064$ μm found in Ref. [47] was used.

We then find, from Eq. (C1), for the *z*-cut quartz in our case,

$$\begin{aligned}|\chi_{\text{eff}}^{(2)}(ssp)|&=1.08\times 10^{-20} \text{ m}^2/\text{V},\\ |\chi_{\text{eff}}^{(2)}(sps)|&=1.12\times 10^{-20} \text{ m}^2/\text{V},\\ |\chi_{\text{eff}}^{(2)}(ppp)|&=0.94\times 10^{-20} \text{ m}^2/\text{V}.\end{aligned} \tag{C4}$$

APPENDIX D: DERIVATION OF EQ. (4.6)

The proof of Eq. (4.6) is quite straightforward. Let us consider the first equation in Eq. (4.6) as an example. We can express Eq. (2.7) in the form

$$(A_s)_{ijk}=N_S\int\sum_{\lambda\mu\nu}(a_s)_{\lambda\mu\nu}(\hat{\lambda}\cdot\hat{i})(\hat{\mu}\cdot\hat{j})(\hat{\nu}\cdot\hat{k})f(\Omega)d\Omega. \tag{D1}$$

Knowing that

$$\sum_{ij}\delta_{ij}(\hat{\lambda}\cdot\hat{i})(\hat{\mu}\cdot\hat{j})=\delta_{\lambda\mu}, \tag{D2}$$

we find

$$\sum_{ij}\delta_{ij}(A_s)_{ijk}=N_S\sum_{\lambda\mu\nu}\delta_{\lambda\mu}(a_s)_{\lambda\mu\nu}\int(\hat{\nu}\cdot\hat{k})f(\Omega)d\Omega. \tag{D3}$$

For the CH_2 symmetric stretch there are only three independent nonvanishing $(a_s)_{\lambda\mu\nu}$ elements $(a_s)_{\xi\xi\xi}$, $(a_s)_{\eta\eta\zeta}$, and $(a_s)_{\zeta\zeta\zeta}$. Therefore, we have

$$\sum_{\lambda\mu}\delta_{\lambda\mu}(a_s)_{\lambda\mu\nu}=\delta_{\nu\zeta}[(a_s)_{\xi\xi\zeta}+(a_s)_{\eta\eta\zeta}+(a_s)_{\zeta\zeta\zeta}]. \tag{D4}$$

Insertion of Eq. (D4) into Eq. (D3) yields

$$\sum_{ij}\delta_{ij}(A_s)_{ijk}=N_S[(a_s)_{\xi\xi\zeta}+(a_s)_{\eta\eta\zeta}+(a_s)_{\zeta\zeta\zeta}]\times\int(\hat{\zeta}\cdot\hat{k})f(\Omega)d\Omega, \tag{D5}$$

which is identical to the first equation in Eq. (4.6) if $\hat{k}=\hat{z}$. Similarly, the other three equations in Eq. (4.6) can be proved.

[1] C. Mauguin, Bull. Soc. Fr. Mineral. Cristallogr. **34**, 71 (1911).
[2] *Liquid Crystals and Uses*, edited by B. Bahadur (World Scientific, Singapore, 1990).
[3] D. W. Berreman, Phys. Rev. Lett. **28**, 1683 (1972); Mol. Cryst. Liq. Cryst. **23**, 215 (1973).
[4] J. M. Geary, J. W. Goodby, A. R. Kmetz, and J. S. Patel, J. Appl. Phys. **62**, 4100 (1987).
[5] W. Chen, M. B. Feller, and Y. R. Shen, Phys. Rev. Lett. **63**, 2665 (1989).
[6] M. B. Feller, W. Chen, and Y. R. Shen, Phys. Rev. A **43**, 6778 (1991).
[7] M. Barmentlo, R. W. J. Hollering, and N. A. J. M. van Aerle, Phys. Rev. A **46**, R4490 (1992).
[8] X. Zhuang, L. Marrucci, and Y. R. Shen, Phys. Rev. Lett. **73**, 1513 (1994).
[9] R. Meister and B. Jérôme, Macromolecules **32**, 480 (1999).
[10] Y. M. Zhu, L. Wang, Z. H. Lu, Y. Wei, X. X. Chen, and J. H. Tang, Appl. Phys. Lett. **65**, 49 (1994).
[11] Y. B. Kim, H. Olin, S. Y. Park, J. W. Choi, L. Komitov, M. Matuszczyk, and S. T. Lagerwall, Appl. Phys. Lett. **66**, 2218 (1995).
[12] A. J. Pidduck, G. P. Bryan-Brown, S. Haslam, R. Bannister, and I. Kitely, J. Vac. Sci. Technol. A **14**, 1723 (1996).
[13] I. Hirosawa, Jpn. J. Appl. Phys., Part 1 **35**, 5873 (1996).
[14] K. Sakamoto, R. Arafune, N. Ito, S. Ushioda, Y. Suzuki, and S. Morokawa, Jpn. J. Appl. Phys. **33**, L1323 (1994); K. Sakamoto, R. Arafune, N. Ito, and S. Ushioda, J. Appl. Phys. **80**, 431 (1996).
[15] R. Hasegawa, Y. Mori, H. Sasaki, and M. Ishibashi, Jpn. J. Appl. Phys. **35**, 3492 (1996).
[16] R. Arafune, K. Sakamoto, and S. Ushioda, Appl. Phys. Lett. **71**, 2755 (1997).
[17] G. D. Hietpas, J. M. Sands, and D. L. Allara, J. Phys. Chem. B **102**, 10 556 (1998).
[18] M. F. Tony, T. P. Russell, J. A. Logan, H. Kikuchi, J. M. Sands, and S. K. Kumar, Nature (London) **374**, 709 (1995).
[19] I. Hirosawa, N. Sasaki, and H. Kimura, Jpn. J. Appl. Phys., Part 2 **38**, L583 (1999).

[20] M. G. Samant, J. Stöhr, H. R. Brown, T. P. Russell, J. M. Sands, and S. K. Kumar, Macromolecules **29**, 8334 (1996).
[21] K. Weiss, C. Wöll, E. Böhm, B. Fiebranz, G. Forstmann, B. Peng, V. Scheumann, and D. Johannsmann, Macromolecules **31**, 1930 (1998).
[22] J. Stöhr, M. G. Samant, A. Cossy-Favre, J. Diaz, Y. Momoi, S. Odahara, and T. Nagata, Macromolecules **31**, 1942 (1998).
[23] A. Cossy-Favre, J. Diaz, Y. Liu, H. R. Brown, M. G. Samant, J. Stöhr, A. J. Hanna, S. Anders, and T. P. Russell, Macromolecules **31**, 4957 (1998).
[24] Y. R. Shen, in *Frontiers in Laser Spectroscopy*, Proceedings of the International School of Physics ''Enrico Fermi,'' Course CXX, edited by T. W. Hänsch and M. Inguscio (North-Holland, Amsterdam, 1994), p. 139.
[25] X. Wei, X. Zhuang, S.-C. Hong, T. Goto, and Y. R. Shen, Phys. Rev. Lett. **82**, 4256 (1999).
[26] In MKS units, there are two different conventions to define $\boldsymbol{\chi}^{(2)}$ and other related quantities depending on whether or not ϵ_0 is included in Eq. (2.1). Note that the convention we choose here is different from the one used in Ref. [25].
[27] Equation (2.2) is valid only if $I(\omega_s)$, $I(\omega_1)$ and $I(\omega_2)$ are defined in vacuum or air. If they are defined in a medium with a dielectric function $\epsilon_1(\omega_i)$, Eq. (2.2) should be modified to (see, for example, Ref. [24])
$$I(\omega_s)=\frac{\omega_s^2|\chi_{\mathrm{eff}}^{(2)}|^2 I(\omega_1)I(\omega_2)}{8\epsilon_0 c^3\cos^2\beta_s\sqrt{\epsilon_1(\omega_s)\epsilon_1(\omega_1)\epsilon_1(\omega_2)}}.$$
[28] Y. R. Shen, *The Principles of Nonlinear Optics* (Wiley, New York, 1984) pp. 23–25.
[29] R. Superfine, J. Y. Huang, and Y. R. Shen, Chem. Phys. Lett. **172**, 303 (1990).
[30] C. Hirose, N. Akamatsu, and K. Domen, J. Chem. Phys. **96**, 997 (1992); C. Hirose, H. Yamamoto, N. Akamatsu, and K. Domen, J. Phys. Chem. **97**, 10 064 (1993).
[31] R. G. Snyder, J. Chem. Phys. **42**, 1744 (1965).
[32] K. B. Wiberg and J. J. Wendolosky, J. Phys. Chem. **88**, 586 (1984).
[33] K. M. Gough, J. Chem. Phys. **91**, 2424 (1989).
[34] S. Krimm, C. Y. Liang, and G. B. B. M. Sutherland, J. Polym. Sci. **22**, 227 (1956).
[35] Y. R. Shen, Appl. Phys. B: Lasers Opt. **68**, 295 (1999).
[36] X. Wei, S.-C. Hong, A. I. Lvovsky, H. Held, and Y. R. Shen, J. Phys. Chem. B **104**, 3349 (2000).
[37] P. Guyot-Sionnest, R. Superfine, J. H. Hunt, and Y. R. Shen, Chem. Phys. Lett. **144**, 1 (1988).
[38] R. K. Iler, *The Chemistry of Silica* (Wiley, New York, 1979), pp. 622–729.
[39] C. S. Marvel and C. E. Denoon, J. Am. Chem. Soc. **60**, 1045 (1938).
[40] D. Zhang, R. S. Ward, Y. R. Shen, and G. A. Somorjai, J. Phys. Chem. B **101**, 9060 (1997).
[41] C. S. Mullin, P. Guyot-Sionnest, and Y. R. Shen, Phys. Rev. A **39**, 3745 (1989).
[42] A. I. Kitaigorodskii, *Organic Chemical Crystallography* (Consultants Bureau, New York, 1961) pp. 322 and 323.
[43] P. Ye and Y. R. Shen, Phys. Rev. B **28**, 4288 (1983).
[44] X. Zhuang, P. B. Miranda, D. Kim, and Y. R. Shen, Phys. Rev. B **59**, 12 632 (1999).
[45] X. Zhuang, D. Wilk, L. Marrucci, and Y. R. Shen, Phys. Rev. Lett. **75**, 2144 (1995).
[46] S. Kobayashi and Y. Iimura, Proc. SPIE **2175**, 122 (1994); D.-S. Seo, K. Araya, N. Yoshida, M. Nishikawa, Y. Yabe, and S. Kobayashi, Jpn. J. Appl. Phys. **34**, L503 (1995).
[47] *Handbook of Lasers*, edited by R. J. Pressley (Chemical Rubber Co., Cleveland, 1971), pp. 489 and 497.
[48] Y. R. Shen, *The Principles of Nonlinear Optics* (Ref. [28]), pp. 73–76.